



UNIVERSITY OF LEEDS

This is a repository copy of *Quantification of mesh induced anisotropy effects in the phase-field method.*

White Rose Research Online URL for this paper:  
<http://eprints.whiterose.ac.uk/84397/>

Version: Accepted Version

---

**Article:**

Mullis, AM (2006) Quantification of mesh induced anisotropy effects in the phase-field method. *Computational Materials Science*, 36 (3). 345 - 353. ISSN 0927-0256

<https://doi.org/10.1016/j.commatsci.2005.02.017>

---

© 2006, Elsevier. Licensed under the Creative Commons Attribution-NonCommercial-NoDerivatives 4.0 International  
<http://creativecommons.org/licenses/by-nc-nd/4.0/>

**Reuse**

Unless indicated otherwise, fulltext items are protected by copyright with all rights reserved. The copyright exception in section 29 of the Copyright, Designs and Patents Act 1988 allows the making of a single copy solely for the purpose of non-commercial research or private study within the limits of fair dealing. The publisher or other rights-holder may allow further reproduction and re-use of this version - refer to the White Rose Research Online record for this item. Where records identify the publisher as the copyright holder, users can verify any specific terms of use on the publisher's website.

**Takedown**

If you consider content in White Rose Research Online to be in breach of UK law, please notify us by emailing [eprints@whiterose.ac.uk](mailto:eprints@whiterose.ac.uk) including the URL of the record and the reason for the withdrawal request.



[eprints@whiterose.ac.uk](mailto:eprints@whiterose.ac.uk)  
<https://eprints.whiterose.ac.uk/>

# Quantification of Mesh Induced Anisotropy Effects in the Phase-Field Method

*A. M. Mullis*

Institute for Materials Research, University of Leeds, Leeds LS2 9JT, UK

## *ABSTRACT*

Phase-field modelling is one of the most powerful techniques currently available for the simulation from first principles the time dependant evolution of complex solidification microstructures. However, unless care is taken the computational mesh used to solve the set of partial differential equations that result from the phase-field formulation of the solidification problem may introduce a stray, or implicit, anisotropy, which would be highly undesirable in quantitative calculations. In this paper we quantify this effect as a function of various computational parameters and subsequently suggest techniques for mitigating the effect of this stray anisotropy.

**PACS:** 81.31.-t, 81.30.Fb, 64.60.-i

**Keywords:** Phase-field method, solidification, crystalline anisotropy

## **Introduction**

The dendrite is a solidification morphology characteristic of many metallic melts and certain other systems with a low entropy of fusion. It is a structure of both great practical and theoretical interest. Dendrites are parabolic needle crystals that develop complex, time dependent shapes, normally as the result of extensive branching which gives rise to a tree-like structure.

During the processing of metallic components, solidification from the parent melt is almost invariably the first step. Remnants of the dendritic microstructures formed during solidification often survive subsequent processing operations, such as rolling and forging, and the length scales established by the dendrite can influence not only the final grain size but also micro- and hence macro-segregation patterns. This can have a wide-ranging influence on both the properties of finished metallic products, affecting for instance mechanical properties, corrosion resistance and surface finish, and on the formability of metallic feedstock, such as the ability to resist hot tearing during rolling.

Theoretical interest stems from the fact the dendrite is a prime example of a pattern forming system where complex morphologies arise from initially homogeneous conditions due to the highly non-linear response of the controlling system. Moreover, although the governing equations for dendritic growth have been known for many decades, finding solutions to the free-boundary problem, even in the tip region has proved enormously complicated. Indeed, finding analytical steady-state solutions for the radius of curvature of the dendrite at its tip has proved to be beyond all orders of perturbation theory [1].

The problem of predicting the operating point of the dendrite first became apparent in 1947 when Ivantsov [2] showed that an isothermal paraboloid of revolution, growing with radius of curvature  $R$  and (tip) velocity  $V$  into an isotropic undercooled melt was a shape preserving solution to the diffusion equation, thus giving rise to the idea of the needle dendrite. However, the Ivantsov analytical solution for such a crystal is degenerate in that it relates the Peclet number, and not the growth velocity, to undercooling, where the Peclet number is defined as

$$P = \frac{VR}{2D_l} \quad (1)$$

where  $D_l$  is the diffusivity in the melt. Consequently, at a given undercooling an infinite set of solutions are admissible, subject to the condition  $VR = \text{constant}$ . Such degeneracy is not observed in nature, where a well-defined growth velocity can always be associated with a given set of initial conditions.

A rigorous approach to the problem of selecting the operating point of a needle crystal is provided by the theory of microscopic solvability [3, 4]. The principal physical insight of solvability theory is that surface tension acts as a singular perturbation which resolves the degeneracy found in the macroscopic problem. Perhaps counter to intuition, it turns out that in the case of an isotropic system the equations have no solution. The principal prediction of solvability theory is that capillary forces break the Ivantsov degeneracy via the relationship

$$R^2V = \frac{2Dd_o}{\sigma^*} \quad (2)$$

where  $d_o$  is the capillary length, which is given by

$$d_o = \frac{\sigma T_m c}{L^2} \quad (3)$$

where  $\sigma$  is the interfacial energy between the solid and liquid phases,  $L$  is the latent heat per unit volume,  $c$  the specific heat per unit volume and  $T_m$  is the equilibrium melting temperature of the solid.  $\sigma^*$  is the anisotropy dependant eigenvalue for the problem, where for a cubic system anisotropy is usually introduced by writing

$$d = d_o(1 - \gamma_d \cos 4\theta) \quad (4)$$

where  $\gamma_d$  is the anisotropy strength. For small Peclet numbers  $\sigma^*$  is found to vary as  $\sigma^*(\gamma_d) \propto \gamma_d^{7/4}$  in the limit  $p, \gamma_d \rightarrow 0$ .

Although it has allowed great advances in our understanding of the steady-state dendritic growth, solvability theory is not suited to the time-dependant growth problem. One of the central advances in the ability to predict non-steady dendritic growth in the last 20 years has been the advent of phase-field modelling. First proposed by Langer [5] and subsequently developed by, among others, Caginalp [6] and Penrose & Fife [7], the basis of the phase-field method is the definition of a phase variable (say  $\phi$ ) the value

of which describes the phase state of the material. At its simplest, for a single-phase solid, this might for instance equate  $\phi \equiv 1$  with the solid and  $\phi \equiv -1$  with the liquid. The central assumption of the phase-field method is that the interface between phases is diffuse, with a finite width  $\delta$ , and that  $\phi$  is thus a continuous variable over the whole domain  $\Omega$  on which the problem is defined. For the simple single-phase system discussed above this would allow  $\phi$  to take values intermediate between the solid and liquid end members, that is  $-1 \leq \phi \leq 1$ . Unlike the classical Stefan problem, in which the solidification front is treated as a mathematically sharp interface at which boundary conditions are applied, the continuity of  $\phi$  over  $\Omega$  allows the equations that govern the evolution of  $\phi$  to be written in a differential form. These are usually derived from either a free-energy or entropy functional which incorporates conservation of energy and positive entropy production, with the Gibbs-Thomson condition relating the local interface temperature to the thermodynamic equilibrium temperature, local interface curvature and interface kinetics. This phase-equation, coupled to a transport equation for either heat or solute, can then be solved using conventional techniques for partial differential equations.

The phase-field method has facilitated significant progress in our understanding of a number of problems associated with time-dependent dendritic solidification including the study of dendritic shapes at high undercoolings [8], a model for spontaneous grain refinement [9] and the inclusion of electric currents through the solidifying material [10]. However, there are a number of problems with the technique, one of which is the implicit anisotropy introduced into the solution by the mesh on which the differential equations are solved. Although most workers in the field recognise this as a potential

pitfall when using phase-field methods the problem has received little systematic study.

The problem arises for the following reasons;

- the finite difference (FD) and finite element (FE) routines generally used to solve the differential phase and transport equations normally discretise the computational domain using a regular mesh. The regularity of the mesh introduces a directionality which is equivalent to an implicit or mesh induced anisotropy to the solution,
- dendritic solidification is very sensitive to small amounts of anisotropy. Consequently, the small level of anisotropy introduced by using FE or FD solvers with a regular mesh can have a significant effect in phase-field simulations when, in many other computational models, this effect would be insignificant.

This work was largely motivated by our observation that mesh induced anisotropy was a far more significant problem in solutal phase-field models than in thermal models. In this paper we set out to systematically analyse the origins of mesh induced anisotropy, accounting for why it is more problematic in solute based systems, to quantify the mesh induced anisotropy as a function of the relevant computational parameters and to suggest mitigating strategies.

### **Computational Model**

Our investigation was conducted using the single-phase model of Warren & Boettinger [11]. As with most phase-field models the basis of the Warren & Boettinger model is the definition of an entropy functional [12, 13], which in this case is

$$S = \int_{\Omega} \left[ s(\phi, e, c) - \frac{1}{2} \bar{\varepsilon}^2 (\nabla \phi)^2 \right] d\Omega \quad (5)$$

where  $s$  is the thermodynamic entropy density,  $\phi$  is the phase variable taking values 0 in the solid and 1 in the liquid,  $e$  is the internal energy density and  $c$  is the concentration of solute (chemical species B) in the solvent (chemical species A). The parameter  $\bar{\varepsilon}$  represents gradient corrections to the entropy density, although gradient corrections to  $c$  and  $e$  are omitted.

It is shown in [11] that in the case of isothermal solidification in an ideal solution between components A and B this lead to an anisotropic phase-equation given by

$$\begin{aligned} \frac{\dot{\phi}}{M_{\phi}} = & \left[ \bar{\varepsilon}^2 \eta^2 \nabla^2 \phi - (1-c)H^A - cH^B \right] - \bar{\varepsilon}^2 \frac{\partial}{\partial x} \left( \eta(\theta) \eta'(\theta) \frac{\partial \phi}{\partial y} \right) \\ & + \bar{\varepsilon}^2 \frac{\partial}{\partial y} \left( \eta(\theta) \eta'(\theta) \frac{\partial \phi}{\partial x} \right) + \bar{\varepsilon}^2 \nabla \cdot \left( \eta^2(\theta) \nabla \phi \right). \end{aligned} \quad (6)$$

Here  $H^A$  and  $H^B$  are defined by

$$H^{A,B}(T, \phi) = W^{A,B} g' + 30 g L^{A,B} \left( \frac{1}{T} - \frac{1}{T_m^{A,B}} \right) \quad (7)$$

where

$$W^{A,B} = \frac{3\sigma^{A,B}}{\sqrt{2}T_m^{A,B}\delta^{A,B}} \quad (8)$$

with  $g$  being the quartic polynomial  $\phi^2(1-\phi)^2$  and  $\delta$  the width of the diffuse interface. In each case the superscripts  $A$  and  $B$  indicate that the specified quantity refers to the pure substances  $A$  and  $B$  respectively. The kinetic mobility is given by

$$M_\phi = (1-c)M^A + cM^B \quad (9)$$

with

$$M^{A,B} = \frac{(T_m^{A,B})^2 \beta^{A,B}}{6\sqrt{2}L^{A,B}\delta^{A,B}} \quad (10)$$

where  $\beta$  is the linear kinetic coefficient for interface attachment in the pure substances  $A$  and  $B$  respectively. Anisotropy has been introduced by writing [14,15]

$$\varepsilon(\theta) = \bar{\varepsilon}\eta(\theta) = \bar{\varepsilon}(1 + \gamma \cos k\theta) \quad (11)$$

where  $\gamma$  is the anisotropy strength,  $k$  is a mode number, which for solidification in a cubic metal will be 4 and

$$\bar{\varepsilon}^{-2} = \frac{6\sqrt{2}\sigma^A\delta^A}{T_m^A} = \frac{6\sqrt{2}\sigma^B\delta^B}{T_m^B} \quad (12)$$

Note that Equation (12) implies that if the surface energies and melting temperatures of species  $A$  and  $B$  are assigned fixed (i.e. physical) values, it is not possible to independently vary both  $\delta^A$  and  $\delta^B$ .

The transport equation is given by

$$\dot{c} = \nabla \cdot D_c \left[ \nabla c + \frac{v_m}{R} c(1-c)(H^B - H^A) \nabla \phi \right] \quad (13)$$

where the effective diffusivity is given by

$$D_c = D_s + p(\phi)(D_l - D_s) \quad (14)$$

with  $v_m$  being the molar mass,  $R$  the gas constant and  $D_s$  the diffusivity in the solid phase.  $p(\phi)$  is a polynomial given by [12]

$$p(\phi) = \frac{\int_0^\phi g(\phi) d\phi}{\int_0^1 g(\phi) d\phi} = \phi^3(10 - 15\phi + 6\phi^2) . \quad (15)$$

The system of differential equations given by Equations (6) and (13) represent a full description of the solidifying system. In this work they have been solved using a simple explicit finite difference method on a uniform square mesh with time step  $\Delta t$  and mesh size  $\Delta t$ . The finite difference scheme employed is first order accurate in  $\Delta t$  and either

second or forth order accurate in  $\Delta x$  (see below), for both the phase and transport equations. The second order scheme uses a 3-point stencil to calculate the differentials, namely

$$T_x = (T_{j+1} - T_{j-1}) / 2(\Delta x) \quad (16)$$

while the forth order scheme uses a 5-point stencil

$$T_x = (T_{j-2} - 8T_{j-1} + 8T_{j+1} - T_{j+2}) / 12(\Delta x) \quad (17)$$

The use of an explicit finite difference scheme means that the time step,  $\Delta t$ , will be limited by a Courant type stability condition. For the transport equation this can be written as

$$\Delta t \leq \frac{(\Delta x)^2}{\zeta D_l} \quad (18)$$

where  $\zeta$  would be exactly 4 in the absence of the non-linear source terms in Equ. (13) and is likely to be  $> 4$  when these terms are present. The equivalent condition for the phase equation is less straightforward, but provided  $M_\phi \mathcal{E}^2 \approx D_l$ , gives a limiting time step comparable to Equ. (18). Consequently we have adopted Equ. (18) as the limiting condition on  $\Delta t$ , where  $\zeta$  is to be determined empirically.

## Determination of the Mesh Induced (Implicit) Anisotropy

In the absence of anisotropy no stable solutions exist for a solid nucleus growing out into its undercooled or supersaturated parent melt. Consequently, an initial circular nucleus will grow to a critical radius, determined usually by the surface energy,  $\sigma$ , before breaking up into random fingers. However, until the critical radius is approached, an initially circular nucleus will, to a very good approximation, retain its circular shape. When anisotropy is present the evolution of the solidifying nucleus is quite different. The solidification velocity will be greater in the direction(s) favoured by the anisotropy so that an initially circular nucleus will rapidly develop a non-circular aspect. In the case of a 4-fold anisotropy this leads rapidly to the development of a ‘rounded off’ square, well before the onset of instability leads to the breakup of the front into fingers. An example of this morphology, with an anisotropy directed towards the sides of the computational domain, is shown in Fig. 1. In order to establish the strength of the implicit anisotropy, at least to first order, we explicitly introduce a counter anisotropy of strength  $\gamma$ , such that a circular aspect is recovered. In the case of a 4-fold anisotropy directed towards the sides of the computational domain, as shown in Fig. 1, the counter anisotropy would also be 4-fold symmetric, but off-set by  $45^\circ$ , that is directed towards the corners of the domain. We thus estimate to first order the strength of the four-fold symmetric component of the mesh induced anisotropy,  $\gamma_{m4}$ .

In order to quantify  $\gamma_{m4}$  a number of simulations have been performed. In all of the simulations performed the parameters used are those given in Table 1, unless stated otherwise. For this parameter set, and using a second order accurate finite difference scheme the measured value of  $\gamma_{m4}$  was 0.025.

## Results

As mentioned above this work was motivated by our observation that mesh induced anisotropy is a far severe problem in solutal models than it is in thermal models. Indeed, we have applied the methodology described above to measure the mesh induced anisotropy in a thermal-phase field model [16, 17] which uses an essentially identical phase equation and found  $\gamma_{m4}$  to be  $< 0.002$ .

Our initial feeling was therefore that the observed difference in the strength of the mesh induced anisotropy was likely to arise from some quantity that differs significantly between thermal and solutal models. The most significant difference between the models is the extent of the diffusion boundary layer ahead of the growing dendrite, which scales with the diffusion coefficient. The ratio  $\alpha_l/D_l$  is typically  $\approx 10^3$  for metals, where  $\alpha_l$  is the thermal diffusivity in the liquid, leading to a comparable ratio for the size of the diffusion boundary layers. In terms of dendritic growth this results in a thermal boundary layer which is typically  $\gg 10R$ , while the extent of the solutal boundary layer is  $< R/10$ . In particular, the small size of the solutal boundary layer may mean that it samples relatively few mesh cells, thus acquiring a directionality that generates an implicit anisotropy within the transport equation. That the mesh induced anisotropy within the solution arises predominantly from the transport equation can be verified by independently varying the order of the solver used for the phase and transport equations. The expectation would normally be that a higher order solver would reduce the mesh induced anisotropy as more mesh points are sampled by the larger stencil employed. The results of this investigation are shown in Table 2. In each simulation the physical parameters used are identical and are as given in Table 1. From

Table 2 it is clear that the transport equation does appear to be the primary source of the mesh induced anisotropy and that increasing the order of the solver does reduce the problem.

In order to establish the dependence of the mesh induced anisotropy as a function of the diffusion boundary layer size we may either vary  $D_l$ , which will alter the physical extent of the boundary layer and hence the number of mesh cells sampled or we may alter  $\Delta x$ , which will keep the physical size of the boundary layer fixed but will include more mesh cells within the fixed physical extent of the boundary layer. In the first instance  $\gamma_{m4}$  was measured as a function of  $D_l$ . During this investigation the ratio  $D_s/D_l$  was held fixed at  $10^{-4}$  and all other quantities were fixed at the values given in Table 1. However, somewhat to our surprise, there was no variation in  $\gamma_{m4}$  despite varying  $D_l$  over a range of two orders of magnitude, from  $10^{-9} \text{ m}^2 \text{ s}^{-1}$  to  $10^{-7} \text{ m}^2 \text{ s}^{-1}$ .

We did, however, find that there was a dependence on the ratio  $D_s/D_l$ , although the not on the particular values assigned to either  $D_l$  or  $D_s$ . Typically  $D_s/D_l$  would be of the order  $10^{-4}$  for substitutional diffusion in metals although for interstitial diffusion this ratio could be as high as  $10^{-1}$ . Figure 2 shows that within the physical range of  $10^{-4} - 10^{-1}$  there is a small drop in  $\gamma_{m4}$ , although if this is extended to the unphysical limit of equal conductivities in the solid and liquid states there is a much more significant drop in the mesh induced anisotropy. However, while the ratio of conductivities in the solid and liquid states does vary significantly between thermal and solutal models it is less clear why this should affect the mesh induced anisotropy than the extent of the diffusion boundary layer.

We subsequently looked therefore at the variation of  $\gamma_{m4}$  with  $\Delta x$ , finding that there was a significant reduction in  $\gamma_{m4}$  as  $\Delta x$  was reduced. However, closer investigation revealed that it was not the number of mesh cells in the diffusion boundary layer that was important, but the number in the diffuse solid-liquid interface. The variation of  $\gamma_{m4}$  with the ratio  $\delta_{\text{int}}/(\Delta x)$ , where  $\delta_{\text{int}}$  is the half-width of the diffuse solid liquid interface is shown in Fig. 3. That it is the ratio  $\delta_{\text{int}}/(\Delta x)$  that is important not the absolute value of  $\Delta x$  was confirmed by independently varying  $\delta_{\text{int}}$  and  $\Delta x$  and obtaining an essentially identical trend when  $\gamma_{m4}$  is plotted against  $\delta_{\text{int}}/(\Delta x)$ . However, this result seems to contradict our earlier findings that the mesh induced anisotropy arises predominantly from the transport equation. Moreover, a mesh induced anisotropy arising within the phase equation would not account for the different behaviour of the thermal and solutal models, as the phase equation, and the way in which it is solved, is very similar between the two models. Consequently we need looked for other ways in which thermal and solutally controlled solidification differ in order to explain these observations.

Another fundamental way in which thermal and solutally controlled solidification differs is that in thermally controlled solidification the temperature is continuous across the solid-liquid interface whereas in solutally controlled solidification the concentration would not, in general, be expected to be continuous at the interface. Rather, it would maintain a constant ratio given by the equilibrium partition coefficient,  $k_e = C_s/C_l$ , where  $C_s$  and  $C_l$  are the solute concentration in at the interface in the solid and liquid phases respectively. This is illustrated schematically in Fig. 4a for a sharp interface model. However, within phase-field this discontinuity in  $c$  is smoothed out over the width of the diffuse interface, such that  $c$  is continuous although  $\nabla c$  may be potentially

very large. In the diffuse interface region  $c$  will sample very few mesh cells, in deed less than in the solute boundary layer, and hence the potential to generate mesh induced anisotropy exists. This would hence explain why  $\gamma_{m4}$  is insensitive to the extent of the solutal boundary layer.

Moreover, it also explains why  $\gamma_{m4}$  shows a dependence on the ratio of the diffusivities in the solid to the liquid states,  $D_s/D_l$ , within the solutal model. As illustrated in Fig. 4b, in the thermal case the thermal diffusivities will typically be of similar magnitude and are often assumed to be identical. For solutally controlled solidification this is not the case with  $D_s/D_l$  typically being around  $10^{-4}$ . As above, in the sharp interface model this results in a discontinuity in  $D_c$  at the interface, but in phase-field this is smoothed out over the width of the diffuse solid-liquid interface, resulting in a potentially large value for  $\nabla D_c$ . Interestingly, the transport equation (13) contain terms in both  $\nabla c$  and  $\nabla D_c$ .

So far we have looked only at the first order component of the mesh induced anisotropy, that having the same 4-fold symmetry as the computational mesh being used to solve the equations and we have described a simple method in which a counter directed 4-fold symmetric anisotropy can be introduced to estimate its magnitude. A further question is whether this 4-fold symmetric component is the only component of the mesh induced anisotropy. This question can be resolved by taking a model in which the 4-fold symmetric component of the mesh induced anisotropy has been exactly cancelled by the explicit anisotropy and allowing it to carry on growing well beyond the limit where the surface instabilities will cause the circular nucleus to break up. If such a simulation shows random branching, the residual (higher order) anisotropy is likely to be

negligible, if it shows a distinct directionality this is probably not the case. One such simulation is shown in Fig. 5, from which a number of observations can be made. The observed branching is clearly not random, and is most likely the result of a small component of anisotropy with 16-fold symmetry,  $\gamma_{m16}$ . Note here that the components directed towards both the sides and the corners of the computational box will have been suppressed by the process used to remove the 4-fold symmetric component of the mesh induced anisotropy. For this reason this method will not reveal any 8-fold symmetric components. The 16-fold symmetric branching has a doublon like characteristic (i.e. a steady narrow channel running down almost the entire length of the trunk) which is indicative of growth at low anisotropy. Consequently, although we have not attempted to quantify the magnitude of the  $\gamma_{m16}$ , it is likely to be small. It is also possible that if the 16-fold symmetric component of the mesh induced anisotropy were cancelled out, components with a yet higher symmetry would be revealed.

## **Discussion**

The results presented here indicate that, conceptually, the simplest way to minimise the implicit computationally induced anisotropy is to ensure that there is a high density of mesh cells within the interface region. However, if a regular meshing is utilised this can rapidly lead to an unmanageably large grid with correspondingly long computation times. One potential route to introducing a very fine grid in the interface region while preserving reasonable computational efficiency over the rest of the domain is the use of adaptive meshing techniques [18, 19, 20], although this is not without its own problems. Dynamically updating the grid around the evolving interface region is a far from trivial matter. Moreover, as the structure of the grid evolves with time, implementation of

such schemes on multi-processor machines requires dynamic load balancing, which tends to limit the gains that can be made moving to large numbers of processors. No such considerations apply to fixed grid computation. Also, due to the highly non-linear nature of the phase equation and the non-linear source terms in the (solute) transport equation, explicit solvers are still widely used in phase-field computations. However, if used in conjunction with adaptive meshing this can give rise to problems with very small time steps being used, as the maximum time step scales with the square of the smallest cell in the mesh. Consequently, for maximum benefit adaptive meshing should be coupled with a fully implicit solver, although this is far from trivial.

Other techniques such as solving on multiple rotated grids or using unstructured meshing could potentially also result in significantly reduced mesh induced anisotropy. In simulations of the competition between kinetic and capillary anisotropy during dendritic growth, Ihle [21] used systems of 2 or 4 mutually rotated, regular finite difference grids to reduce the mesh induced anisotropy. However, this was for a sharp interface, front tracking, computational scheme. We are not aware of any application of this technique to phase-field modelling, although there does not seem to be any reason why it should not, in principle, be possible. Where the system of equations is solved using finite elements, employing an irregular meshing without a strong directionality is likely to significantly reduce the problem computationally induced anisotropy. For an explicit time-stepping fixed mesh finite element (FE) methods are likely to be rather inefficient compared to a finite difference (FD) scheme with similar resolution. However, if an implicit solver is used or mesh adaptivity is introduced, the efficiency of FE and FD schemes is likely to be much closer. Phase-field simulations of particle

coalescence utilising a refined finite element mesh without a strong directional structure have been conducted by Burman *et al.* [22]. Although they do not explicitly check whether there is any mesh induced anisotropy, their results on the growth and subsequent coalescence of initially spherical particles would suggest that mesh induced effects in their computational scheme are very small. However, the down side of their scheme is that to refine the grid in the region of the solid-liquid interface requires remeshing of the entire domain. In their reported results most simulations required  $\approx 50$  new meshes to be generated, although in the most extreme case over 650 remeshings were conducted.

A potential alternative strategy for the removal of mesh induced anisotropy would be to eliminate the mesh altogether (at least for the transport equation), by using a Monte Carlo algorithm to integrate the transport equation. Such a strategy has been implemented by Plapp & Karma [23, 24] who use a large number of random walkers to find solutions to the transport equation thus coping efficiently with the disparity in length scales between the diffusion field and the dendrite tip radius for pure thermal solidification at very low undercoolings. However, as implemented by these authors, the scheme was only used to solve the far-field problem well away from the solid-liquid interface region. Close to the interface region a standard finite difference scheme was employed. Consequently, as implemented in [23, 24] the use of random walkers to integrate the transport equation would have little effect on mesh induced anisotropy, although it may, in principal, be possible to implement the Monte Carlo algorithm over the whole domain.

Finally, although the main concern of this paper has been a particular class of phase-field models (those derived from the Wheeler, Boettinger & Mc Fadden (WBM) [13] formulation), there are a range of formulations of the phase-field technique. It may therefore be appropriate to mention the role of mesh induced anisotropy in other formulations of the problem and indeed in some related techniques for solving the dendritic growth problem, in particular the level set method, which has some formal similarities with phase-field.

Perhaps the most significant alternative formulation of the phase-field technique to the model we have discussed above is the thin-interface model, which has been developed extensively by Karma & co-workers [25, 26, 27]. Developed initially [25, 26] as a tool for probing the agreement between phase-field & microscopic solvability models [28] of solidification in the important regime of very low undercoolings at which experiments on analogue systems such as succinonitrile [29] can be conducted, the thin interface model has two distinct differences from the model discussed above. Firstly, a judicious choice of computational parameters allows for the elimination of interface kinetic effects and secondly, unlike the WBM formulation, the time-step to be used for the phase equation is independent of the diffuse interface width,  $\delta$ . As far as we are aware, mesh induced anisotropy has not been the subject of any quantitative investigation in thin interface phase-field models, although solutal versions of the formulation [27, 30] are known to suffer from spurious interface effects. In particular, the magnitude of the (physical) solute trapping effect is significantly overestimated in the thin interface model, an artefact which at present is dealt with by adding in anti-solute trapping terms in a rather *ad hoc* manner [31]. Therefore, given that thin

interface models suffer problems with the jump in the solute profile at the interface we would not be surprised to find they suffered from mesh induced anisotropy effects similar to those described above for WBM type models, although this is not certain.

The level set method, like phase-field, employs implicit tracking of the free boundary in order to handle the complex topology of the solid-liquid interface that may arise during crystallization. In both methods this is achieved by defining as phase variable,  $\phi$ , the value of which defines the phase of the material. The difference with the level set method is that the contour  $\phi \equiv 0$  defines the exact position of the interface (where typically  $\phi > 0$  in the liquid and  $\phi < 0$  in the solid). As such this is a sharp interface model, with the interface dividing the computational domain into separate regions. The transport equation is solved separately in each region, with boundary conditions which are applied at the edges of the computational domain and on the free boundary, while (for thermal growth) a condition of the form

$$cD[\hat{\mathbf{n}}(\nabla T)_l - \hat{\mathbf{n}}(\nabla T)_s] = -Lv_n \quad (19)$$

is applied directly at the locus of  $\phi \equiv 0$ . Here  $c$  the specific heat per unit volume,  $\hat{\mathbf{n}}$  is the outward pointing unit normal to the solid-liquid interface,  $v_n$  is the local velocity of the interface along  $\hat{\mathbf{n}}$  and the subscripts  $l$  and  $s$  relate to the solid and liquid regions of the domain respectively. In addition, a Gibbs-Thomson condition relating the temperature of the interface to its local curvature and velocity may also be applied. The level set method has been applied to the dendrite growth problem by a number of authors [32, 33] and the technique is potentially very exciting as it removes the problems

associated with the diffuse interface used in phase-field methods. However, it is fair to say that the application of the technique is far less well developed than phase-field, with models generally being restricted to single phase, thermally controlled solidification. In contrast multiphase, multicomponent phase-field models are now widespread (see e.g. [34] for a review). Grid induced effects in the level set method are mentioned by Gibou *et al.* [35], who claim that the implicitly introduced anisotropy is likely to be negligible in their model. Certainly, the effects described by us above should not be present in a sharp interface model. However, the ground for their assertion is a pair of simulations in which an 8-fold symmetric seed with branches pointing towards the sides and corners of their computational domain is allowed to grow under a 4-fold symmetric anisotropy. In one case this is directed towards the sides of the domain in the other case towards the corners. The authors' assertion of low implicit anisotropy is based on their observation that the resultant simulated morphologies are similar except for a rotation of  $\pi/4$ . In fact, this is likely to be a fairly insensitive test of implicit anisotropy and their assertion is also somewhat inconsistent with their own results. In simulations performed with an isotropic surface tension they produced a number of doublet-like morphologies. However, the primary growth direction for these was aligned along the co-ordinate axes, clearly indicating a mesh induced effect. Moreover, the doublet is a low, but not zero, anisotropy morphology. For sufficiently low anisotropy the expected morphology would be fractal-like dendritic seaweed.

It would therefore seem to us that, although the details of the mechanisms may be different, mesh induced anisotropy effects are a potential hazard in computational simulations of dendritic solidification, irrespective of the simulation methodology

employed. Consequently, considerable care needs to be exercised, particularly when studying the behaviour of inherently low anisotropy systems.

## **Summary & Conclusions**

Phase-field modelling is one of the most powerful techniques currently available for the simulation from first principles of solidification microstructures. Yet there is an inherent problem that the nature, and indeed existence, of steady-state solutions is dependant on a small parameter, namely the crystalline anisotropy. Moreover, the effective value of this parameter can be influenced by the computational mesh used to solve the set of partial differential equations that result from the phase-field formulation of the problem.

In this paper we have demonstrated that this problem is far more acute for the solidification of alloys than it is for the solidification of pure systems, where the mesh induced anisotropy is barely detectable. In contrast, in solutal systems the mesh induced anisotropy can be comparable to the explicit anisotropy, particularly if the problem is not carefully posed. This mesh induced anisotropy has been quantified above as a function of the diffuse interface width and of the ratio of conductivities in the solid and liquid states. Moreover, by independently varying the order of the solver employed for the transport and phase equations we have been able to demonstrate that the primary source of the mesh induced anisotropy is the transport and not the phase equation. A self consistent explanation of this, and the lack of a significant mesh induced anisotropy in thermal solidification models, is that the anisotropy arises due to the 'jump' in the solute concentration across the solid-liquid interface. In a sharp

interface model this would be a discontinuous change in  $c$  at the interface. However, in phase-field, the assumption of a diffuse solid-liquid interface smooths out the discontinuity over the width of the diffuse interface. Within the interface region very large values of  $\nabla c$  are generated in the transport equation. As potentially very few mesh cells are sampled within the interface region this appears to introduce a directionality in the solution which is manifest as an implicit, or mesh induced, component of the anisotropy,  $\gamma$ . A similar effect is also seen in relation to the discontinuity in the diffusivity of the solid and liquid states across the interface.

Interestingly, even for a simple finite difference scheme employing a regular square meshing, although the dominant component of the mesh induced anisotropy has 4-fold symmetry, there are components with a higher order symmetry. This means that cancelling the effect of the mesh induced with a counter directed explicit anisotropy is unlikely to result in a genuinely isotropic system, although the magnitude of the mesh induced anisotropy can be reduced in this manner. Consequently, where the effect of the mesh induced anisotropy is likely to be important, for instance in the simulation of low anisotropy structures, techniques for the minimisation of mesh induced effects need to be considered.

## References

- [1] E. Brener & D. Temkin, *Phys. Rev. E* **51** (1995), 351.
- [2] G.P. Ivantsov, *Doklady Akademii Nauk SSSR* **58** (1947) 567.

- [3] D.A. Kessler, J. Koplik & H. Levine, *Adv. Phys.* **37** (1988), 255.
- [4] Y. Pomeau & M. Ben-Amar, in ‘Solids far from equilibrium’ pp. 365-431, Cambridge University Press, 1992.
- [5] J.S. Langer, in ‘Directions in condensed matter physics’ (eds. G. Grinstein & G. Mazenko), 1986, pp. 164-186, World Science.
- [6] G. Caginalp, *Phys. Rev. A* **39** (1989) 5887.
- [7] O. Penrose & P.C. Fife, *Physica D* **43** (1990) 44.
- [8] R. Gonzalez-Cinca, *Physica A* **414** (2002) 284.
- [9] A.M. Mullis & R.F. Cochrane, *Acta Mater.* **49** (2001) 2205.
- [10] L.N. Brush, *J. Cryst. Growth* **247** (2003) 587.
- [11] J.A. Warren & W.J. Boettinger, *Acta Metall. Mater.* **43** (1995), 689.
- [12] S.-L. Wang, R.F. Sekerka, A.A. Wheeler, B.T. Murray, S.R. Coriell, R.J. Braun & G.B. McFadden, *Physica D* **69** (1993), 189.
- [13] A.A. Wheeler, W.J. Boettinger & G.B. McFadden, *Phys. Rev. A* **45** (1992) 7424.
- [14] R. Kobayashi, *Physica D* **63** (1993) 410.
- [15] A.A. Wheeler, B.T. Murray & R.J. Schaefer, *Physica D* **66** (1993), 243.
- [16] A.M. Mullis, *Acta Mater.* **51** (2003) 1959
- [17] A.M. Mullis, *Phys. Rev. E* **68** (2003) 011602.
- [18] R.J. Braun & B.T. Murray, *J. Cryst. Growth* **174** (1997) 41.
- [19] N. Provatas, N. Goldenfeld & J. Dantzig, *J. Comput. Phys.* **148** (1999) 265.
- [20] R. Tonhardt & G. Amberg, *J. Cryst. Growth* **213** (2000) 161.
- [21] T. Ihle, *Eur. Phys. J. B* **16** (2000) 337.
- [22] E. Burman, A. Jacot & M. Picasso, *J. Comp. Phys.* **195** (2004) 153.
- [23] M. Plapp & A. Karma, *Phys. Rev. Lett.* **84** (2000) 1740.

- [24] M. Plapp & A. Karma, *J. Comp. Phys.* **165** (2000) 592.
- [25] A. Karma & W.-J. Rappel, *Phys. Rev. E.* **53** (1996) R3017.
- [26] A. Karma & W.-J. Rappel, *J. Cryst. Growth* **174** (1997) 54.
- [27] A. Karma, *Phys. Rev. Lett.* **87** (2001) 115701.
- [28] D.A. Kessler, J. Koplik & H. Levine, *Adv. Phys.* **37** (1988) 255.
- [29] M.B. Koss, J.C. LaCombe, L.A. Tennenhouse, M.E. Glicksman & E.A. Winsa, *Metall. Mater. Trans. A* **30** (1999) 3177.
- [30] S.G. Kim, W.T. Kim & T. Suzuki, *Phys. Rev. E.* **60** (1999) 7186.
- [31] S.G. Kim & W.T. Kim, Oral presentation at Euromat 2003, 1-4 Sept. 2003, Lausanne Ch., Symposium S1.
- [32] S. Chen, B. Merriman, S. Osher & P. Smereka, *J. Comp. Phys.* **135** (1997) 8.
- [33] Y. -T. Kim, N. Goldenfeld & J. Dantzig, *Phys. Rev. E* **62** (2000) 2471.
- [34] W.J. Boettinger, J.A. Warren, C. Beckermann & A. Karma, *Ann. Rev. Mater. Res.* **32** (2002) 163.
- [35] F. Gibou, R. Fedkiw, R. Caflisch & S. Osher, *J. Sci. Comp.* **19** (2003) 183.

## Figure Captions

**Fig. 1.** Schematic diagram showing the morphology of an initial circular nucleus (dotted) as it grows out under the influence of a mesh induced anisotropy directed towards the sides of the computational domain (solid). Also shown is the near circular growth morphology (dashed) after a correcting counter anisotropy directed towards the corners of the computational domain has been introduced. The region shown corresponds to an area  $(\approx 200\Delta x)^2$ , where  $\Delta x = 4.6 \times 10^{-9}$  m, as given in Table 1. This is around half the computational domain actually used in the simulations.

**Fig. 2.** The 4-fold component of the mesh induced anisotropy,  $\gamma_{m4}$ , as a function of the ratio of the solute diffusivities in the solid and liquid states.

**Fig. 3.** The 4-fold component of the mesh induced anisotropy,  $\gamma_{m4}$ , as a function of the ratio of the diffuse interface width to the mesh cell size. The dashed line is the least squares best fit power law curve, the exponent being  $\approx -2.6$ .

**Fig. 4.** Schematic diagram illustrating important differences between thermally controlled and solutally controlled solidification; (a) that in the thermal case the diffusing species is continuous across the solid-liquid interface while in the solutal case it is discontinuous, with a fixed ratio between  $C_s$  and  $C_l$  given by the equilibrium partition coefficient and (b) that in the thermal case the diffusivity is (approximately) continuous across the solid-liquid interface while in the solutal case it is discontinuous. In fact the thermal diffusivity in most metals is higher in the solid state than in the

liquid, typically be a factor of 1.1-2.5, as indicated by the dashed line. However, computationally these are often assumed to be identical.

**Fig. 5.** Growth morphology of from a simulation in which the 4-fold symmetric component of the mesh induced anisotropy has been removed to reveal a small 16-fold symmetric component. Note that the procedure used to remove the 4-fold symmetric component would mask the presence of an 8-fold symmetric component, which may also be present.

**Table I.** Computational and materials parameters used in the simulations reported in this work.

**Table II.** The 4-fold component of the mesh induced anisotropy,  $\gamma_{m4}$ , as a function of the order of the solver employed on the transport,  $O(C)$ , and phase,  $O(\phi)$ , equations.

**Table I**

Quantity	Symbol	Value	Units
Initial alloy concentration	$C_o$	0.408	-
Temperature of liquid	$T_o$	1574	K
Liquidus temperature A	$T_m^A$	1728	K
Liquidus temperature B	$T_m^B$	1358	K
(Volume) latent heat A	$L^A$	$2.35 \times 10^9$	$\text{J m}^{-3}$
(Volume) latent heat B	$L^B$	$1.73 \times 10^9$	$\text{J m}^{-3}$
Interfacial energy A	$\sigma^A$	0.37	$\text{J m}^{-2}$
Interfacial energy B	$\sigma^B$	0.29	$\text{J m}^{-2}$
Kinetic coefficient A	$\beta^A$	$3.3 \times 10^{-3}$	$\text{m s}^{-1} \text{K}^{-1}$
Kinetic coefficient B	$\beta^B$	$3.9 \times 10^{-3}$	$\text{m s}^{-1} \text{K}^{-1}$
Diffusivity in the liquid	$D_l$	$10^{-9}$	$\text{m}^2 \text{s}^{-1}$
Ratio of diffusivities	$D_s/D_l$	$10^{-4}$	
Molar volume	$v_m$	$7.42 \times 10^{-6}$	$\text{m}^3 \text{mol}^{-1}$
Mesh cell size	$\Delta x$	$4.6 \times 10^{-9}$	m
Interface width parameter	$\delta^A$	$1.96 \times 10^{-8}$	m
Time step parameter	$\zeta$	10	
Radius of initial nucleus		$40 \times 10^{-9}$	m

**Table II**

$O(C)$	$O(\phi)$	$\gamma_{m4}$
2	2	0.025
2	4	0.026
4	2	0.009
4	4	0.010

**Figure 1**

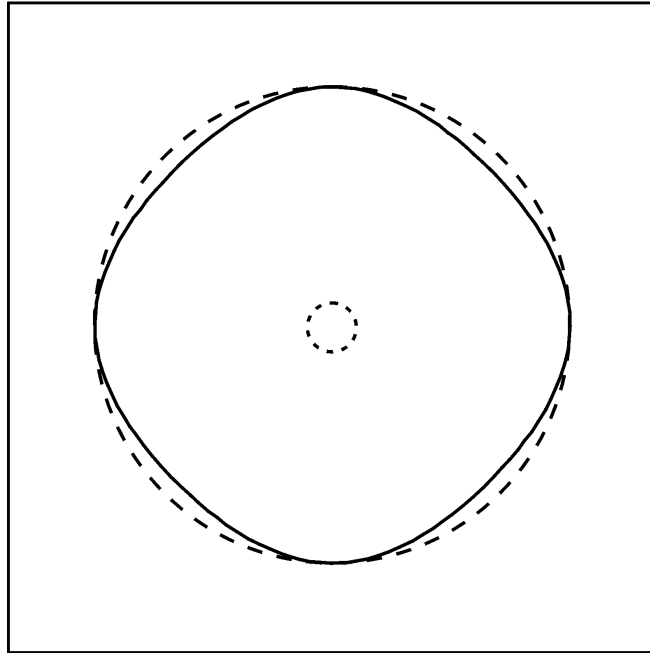


**Figure 2**

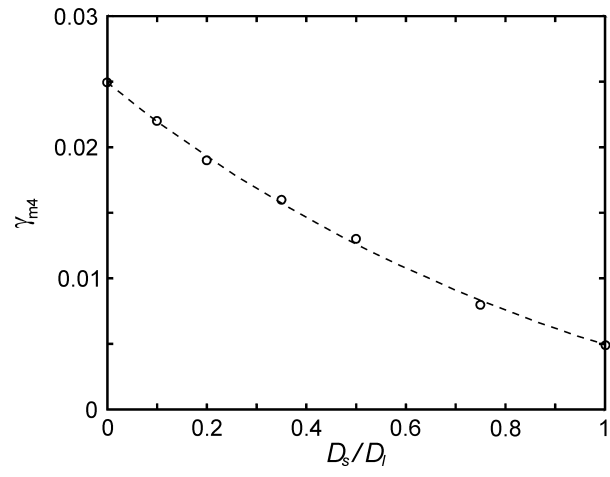


**Figure 3**

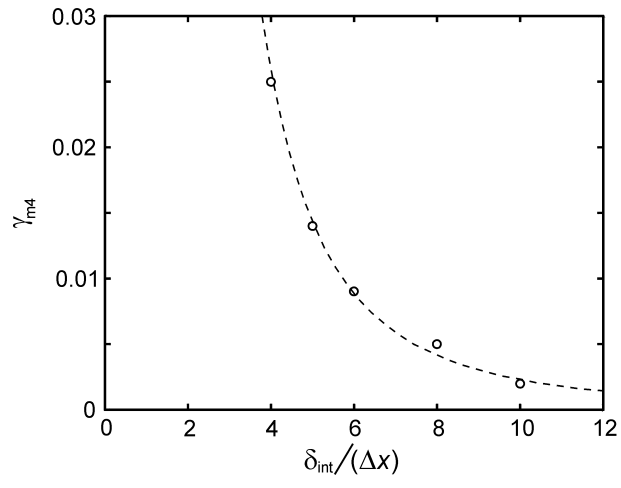


Figure 4a

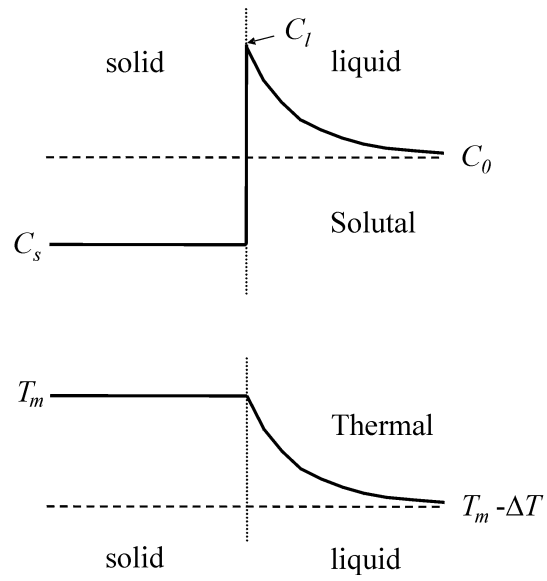
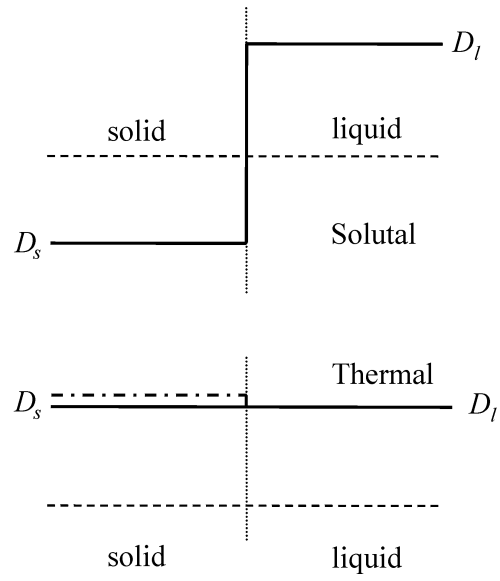


Figure 4b



**Figure 5**

